Research Article

Low-Light Image Enhancement Based on Guided Image Filtering in Gradient Domain

Xiankun Sun,[1,2] Huijie Liu,[2] Shiqian Wu,[3] Zhijun Fang,[2] Chengfan Li,[1] and Jingyuan Yin[1,4]

[1]*School of Computer Engineering and Science, Shanghai University, Shanghai, China*
[2]*School of Electronic and Electrical Engineering, Shanghai University of Engineering Science, Shanghai, China*
[3]*School of Machinery and Automation, Wuhan University of Science and Technology, Wuhan, China*
[4]*Earthquake Administration of Shanghai, Shanghai, China*

Correspondence should be addressed to Xiankun Sun; xksun@sues.edu.cn and Jingyuan Yin; 1061233142@qq.com

We propose a novel approach for low-light image enhancement. Based on illumination-reflection model, the guided image filter is employed to extract the illumination component of the underlying image. Afterwards, we obtain the reflection component and enhance it by nonlinear functions, sigmoid and gamma, respectively. We use the first-order edge-aware constraint in the gradient domain to achieve good edge preserving features of enhanced images and to eliminate halo artefact effectively. Moreover, the resulting images have high contrast and ample details due to the enhanced illumination and reflection component. We evaluate our method by operating on a large amount of low-light images, with comparison with other popular methods. The experimental results show that our approach outperforms the others in terms of visual perception and objective evaluation.

1. Introduction

Video surveillance is now widely used in various fields, like public security, transportation, and so on. The surveillance systems are required to perform not only in day time but also in night time. However, the videos captured in some situations such as dark place or night are very poor so that the objects can hardly be perceived by humans. Thus, it is necessary to enhance the low-light images in image processing and video surveillance.

Recently, the technique of low-light image enhancement has made remarkable progress. The commonly used methods include dark channel prior model [1, 2], neural network model [3, 4], histogram equalization (HE) [5, 6], image fusion [7, 8], wavelet domain algorithm [9, 10], and illumination-reflection model [11–14]. It is noted that the adaptability of dark channel prior model is poor in disposing the images with rich details and high brightness [2]. The design and use of neural network require domain knowledge so that the underlying neural system has good generalization. The idea of histogram equalization is to merge several bins of grayscales in order to increase contrast, but such process may yield detail

loss. The image fusion method needs multiple frame images, which is not applicable for single image frame. Wavelet transform is alternative technique for low-light image enhancement as shown in [9]. The most popular method in enhancing low-light images is to decompose images with the illumination-reflection model.

It was proposed by Land [15] that an image $J(x, y)$ can be decomposed by the reflection component $R(x, y)$ and the illumination component $L(x, y)$:

$$J(x, y) = R(x, y) \cdot L(x, y), \tag{1}$$

where (x, y) represents the coordinates of image. Normally, the illumination component is determined by the dynamic range of the underlying image, while the reflection component is dependent on the intrinsic characteristics of the objects within the underlying image. Equation (1) is generally converted to the logarithmic domain so that the multiplication becomes addition.

The illumination component can be obtained by various methods, such as multiscale Gaussian function in [11], an improved Gaussian function in [12], and the bilateral
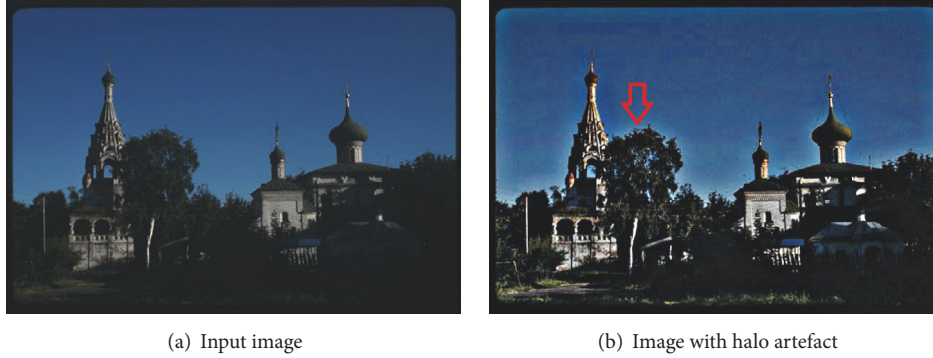
(a) Input image

(b) Image with halo artefact

FIGURE 1: Halo artefact.

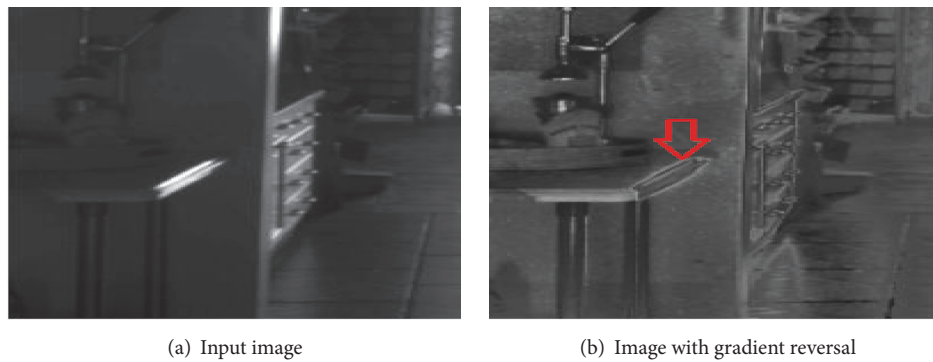(a) Input image

(b) Image with gradient reversal

FIGURE 2: Gradient reversal.

filtering-based method in [14]. The key idea behind the Gaussian function is to use a low-pass filter as shown in (2). In the equation, $F(x, y)$ represents a center-around function, which is also a low-pass filter, and the symbol $*$ represents the convolution. Then, the reflection component can be obtained from (3) with the illumination component.

$$L(x, y) = F(x, y) * J(x, y), \qquad (2)$$

$$\lg[R(x, y)] = \lg[J(x, y)] - \lg[L(x, y)]. \qquad (3)$$

While calculating the illumination component and the reflection component of an image, what is most important is edge preserving and making the flat region smooth. The Multiscale Retinex (MSR) algorithm in [11] processes each color channel individually and then removes the illumination component to keep reflection component. Such processing is liable to color distortion. In addition, the method cannot achieve edge preserving and easily yields halo artefact as shown in Figure 1(b). Bilateral filtering (BLF), proposed by Tomaci and Mabduchi [16], is a good method for edge preserving and eliminating halo artefact. It was pointed out in [17] that the BLF may result in gradient reversal as shown in Figure 2(b). Accordingly, guided image filter (GIF) [17] and its variants, that is, weighted guided image filter (WGIF) [18] and guided image filter in gradient domain (GDGIF) [19] were proposed to achieve good edge preserving.

In this paper, we present a new method for low-light image enhancement, which mainly contributes to the following three aspects: (1) In order to effectively cope with the halo artefact and gradient reversal, the proposed method uses the illumination-reflection model and selects the GIF in gradient domain characterized by smoothness and edge preserving to estimate the illumination component; (2) the proposed method works on HSI color space to eliminate color distortion; (3) the illumination component and the reflection component are enhanced by nonlinear sigmoid and gamma transforms, respectively, to improve image contrast and enhance image details.

The remainder of the paper is organized as follows: Section 2 depicts the proposed low-light image enhancement algorithm. Section 3 demonstrates experimental results, followed by conclusion drawn in Section 4.

2. The Proposed Approach

The proposed method for enhancing low-light images consists of the following steps:

(1) Converting the low-light image from RGB color space to HSI color space

(2) For intensity (illumination) layer, estimating the illumination component with guided image filter in

gradient domain, followed by extracting the reflection component

(3) Enhancing the illumination component with a nonlinear sigmoid transform

(4) Enhancing the reflection component with a nonlinear gamma transform

(5) Taking the antilog of the sum of steps (3) and (4) as the enhanced intensity layer

(6) Converting the new HSI image back to RGB, which produces the final enhanced image

2.1. Guided Image Filter in Gradient Domain.

GDGIF [19] and WGIF [18] are both the improvements of the guided image filter. Basically, the output image q_i is a linear transform of guided image g_i in a square window M_k centered at the pixel k:

$$q_i = a_k g_i + b_k, \quad \forall i \in M_k. \tag{4}$$

In (4), guided image g_i can be input image p_i itself. The pixel i is located in the window M_k of length $(2r + 1)$, in which r is filter radius. a_k and b_k are linear coefficients in pixel k. For GIF, WGIF, and GDGIF, the larger value of a_k implies better edge preserving. On the contrary, if the value of a_k is much closer to 0, the filters have good smoothing performance in flat regions.

According to the gradient-domain optimization framework in [20], the task of filtering an image means converting one input image p_i into the final image q_i, which can be expressed as an energy function $E(a_k, b_k)$ including the zero-order data cost function $E_d(i)$ and first-order gradient cost function $E_g(i)$ terms:

$$E(a_k, b_k) = \sum_{i \in M_k} \left(E_d(i) + E_g(i) \right), \tag{5}$$

$$E_d(i) = (a_k g_i + b_k - p_i)^2, \tag{6}$$

$$E_g(i) = \varphi(i) \left\| \nabla q_i \right\|^2, \tag{7}$$

where $\|\nabla q_i\|$ is gradient magnitude; $\varphi(i)$ is gradient weight constraint. In (4), the gradient magnitude of q_i is $\|\nabla q_i\| = a_k$.

2.1.1. Guided Image Filter.

In the guided image filter [17], $\varphi_1(i) = \varepsilon$, the expressions of a_k and b_k can be obtained according to (4)–(7) shown as follows:

$$a_k = \frac{(1/|w|) \sum_{k:i \in M_k} g_i p_i - \mu_k \overline{p_k}}{\sigma_k^2 + \varepsilon}, \tag{8}$$

$$b_k = \overline{p_k} - a_k \mu_k,$$

where μ_k is the mean of image g_i in the window M_k, and σ_k^2 is the variance of image g_i in the window M_k, $|w|$ is the total pixel number in window M_k, and $\overline{p_k}$ is the mean of image p_i in window M_k. ε is a regularization parameter, which controls the trade-off between edge preserving and smoothness. As ε is generally fixed ratherthan spatially varying in filtering process, halo artefact is unavoidable in edges.

2.1.2. Weighted Guided Image Filter.

Li et al. [18] proposed the WGIF, where a spatially varying gradient weight constraint $\varphi_2(i) = \varepsilon / \Gamma_{g\_k}$ was added in (7).

$$\Gamma_{g\_k} = \frac{1}{N} \sum_{i=1}^{N} \frac{\sigma_{g,1}^2(k) + \lambda}{\sigma_{g,1}^2(i) + \lambda}, \tag{9}$$

where Γ_{g_k} is a single-scale edge-aware weighting, which is defined by using local variances in 3×3 windows, $\sigma_{g,1}^2(k)$ is the variance of guided image g_i in the 3×3 window, N is the number of image pixels, λ is a small constant and its value is $(0.001 \times L)^2$, and L is the dynamic range of the input image. The expressions of a_k' and b_k' in the WGIF can be obtained according to (4)–(7) as shown below:

$$a_k' = \frac{(1/|w|) \sum_{k:i \in M_k} g_i p_i - \mu_k \overline{p_k}}{\sigma_k^2 + \varepsilon / \Gamma_{g\_k}}, \tag{10}$$

$$b_k' = \overline{p_k} - a_k' \mu_k.$$

It is noted that the edge-aware weighting Γ_{g_k} is spatially varying in the WGIF; that is, Γ_{g_k} is larger than 1 when the pixel k locates in the edge area, and Γ_{g_k} is smaller than 1 when the pixel k locates in the flat area. As a result, a_k' is closer to 1 than a_k in the GIF, which implies that WGIF has the better edge preservation than GIF.

WGIF can reduce the halo artefact to some extent. However, both the GIF and the WGIF filters have no explicit constraints to cope with edges. Both cannot preserve edges well because image filtering is performed on edges, which definitely smoothed the edges [19, 21].

2.1.3. Guided Image Filter in Gradient Domain.

Kou et al. [19] proposed the guided image filter in gradient domain (GDGIF), by adding an explicit first-order (gradient domain) edge-aware constraint $E_e(i)$ to gradient-domain equation (5) shown below:

$$E(a_k, b_k) = \sum_{i \in M_k} \left(E_d(i) + E_g(i) + \phi E_e(i) \right), \tag{11}$$

$$E_e(i) = \alpha \left\| \nabla q_i - \nabla p_i \right\|^2,$$

where $E_e(i)$ is edge-aware constraint. The aim is to perceive the changes in local neighbourhoods so that the similar filtering is performed in the similar regions. α is a weight value, ∇q_i and ∇p_i represent the gradient values of output image q_i and input image p_i.

In the GDGIF, a multiscale edge-aware varying spatially gradient weight constraint $\varphi_3(i) = \varepsilon / \widehat{\Gamma}_{g\_k}$ is added in (7). The energy function of GDGIF is shown in (12), in which the

(a) Original image   (b) Edge results by Γ_{g_k} (c) Edge results by $\widehat{\Gamma}_{g\_k}$
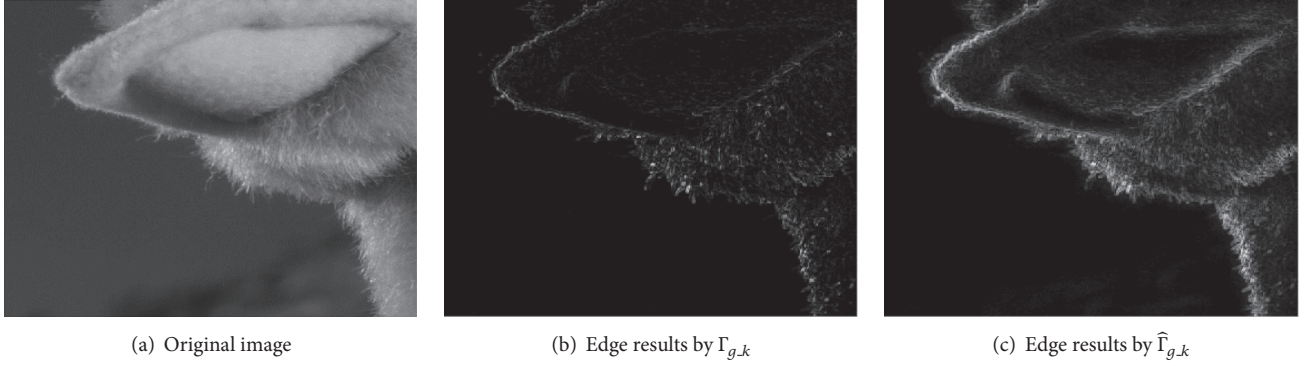
Figure 3: Comparison of $\widehat{\Gamma}_{g\_k}$ and Γ_{g_k}.

second item is the combination of the first-order gradient cost function $E_g(i)$ and the edge-aware constraint $E_e(i)$.

$$E\left(a_k'', b_k''\right)$$
$$= \sum \left(\left(a_k'' g_i + b_k'' - p_i\right)^2 + \frac{\varepsilon}{\widehat{\Gamma}_{g\_k}} \left(a_k'' - \gamma_k\right)^2 \right), \tag{12}$$

$$\widehat{\Gamma}_{g\_k} = \frac{1}{N} \sum_{i=1}^{N} \frac{\chi_k + \lambda}{\chi_i + \lambda}, \tag{13}$$

$$\gamma_k = 1 - \frac{1}{1 + e^{\eta(\chi_k - \mu_{\chi,\infty})}}, \tag{14}$$

where $\widehat{\Gamma}_{g\_k}$ is defined by local variances of $(2r + 1) \times (2r + 1)$ windows of all pixels; r is the filter radius. It is noted that $\widehat{\Gamma}_{g\_k}$ is a multiscale edge-aware weighting varying spatially, in which $\chi_k = \sigma_{g,1}(k) * \sigma_{g,r}(k)$. The edge-aware weighting detects the edge more accurately, and a pixel is detected as an edge pixel when the two scale variances are very large.

The comparison of $\widehat{\Gamma}_{g\_k}$ and Γ_{g_k} in WGIF of an image is shown in Figure 3. The edges of the image are detected accurately by using the multiscale edge-aware weighting $\widehat{\Gamma}_{g\_k}$ rather than using the single-scale edge-aware weighting Γ_{g_k} in WGIF.

In (14), γ_k is an edge-aware constraint to preserve edges. $\mu_{\chi,\infty}$ is the mean of all χ_i, and the value of η is $4/(\mu_{\chi,\infty} - \min(\chi_i))$. The value of γ_k is close to 1 when the pixel k locates in the edge area, and the value is close to 0 when the pixel k locates in the flat area.

The expressions of a_k'' and b_k'' in the GDGIF can be obtained according to (12)–(14), shown as follows:

$$a_k'' = \frac{(1/|w|) \sum_{k:i \in M_k} g_i p_i - \mu_k \overline{p_k} + \left(\varepsilon/\widehat{\Gamma}_{g\_k}\right) \gamma_k}{\sigma_k^2 + \varepsilon/\widehat{\Gamma}_{g\_k}}, \tag{15}$$

$$b_k'' = \overline{p_k} - a_k'' \mu_k.$$

When the input image p_i and guided image g_i are the same, the GDGIF has better edge preserving and smoother

features than the GIF and the WGIF due to the following two points.

(1) When pixel k locates in the edge area, the expression of a_k'' can be computed as

$$a_k'' = \frac{\sigma_k^2 + \left(\varepsilon/\widehat{\Gamma}_{g\_k}\right) \gamma_k}{\sigma_k^2 + \varepsilon/\widehat{\Gamma}_{g\_k}}. \tag{16}$$

It is seen that the value of γ_k is 1, and the value of a_k'' is 1, which is independent of parameter ε. In fact, the value of a_k'' in GDGIF is much closer to 1 than it is in GIF and WGIF. Hence, GDGIF has the best edge preserving feature.

(2) When a pixel k locates in the flat areas, the value γ_k is close to 0, the parameter a_k'' is accordingly independent of the choice of ε. As a result, we can select larger ε in GDGIF than that in WGIF and GIF, so that better smoothing is achieved without affecting the edge preserving [19].

For example, we use GIF, WGIF, and GDGIF for image filtering by choosing the same filter radius $r = 16$ and regularization parameter $\varepsilon = 0.8^\wedge 2$. The result is shown in Figure 4. It is observed that the image filtered by GDGIF has the best edge preserving.

In summary, the GDGIF has the best edge preserving and smoothing features. As a result, we choose the GDGIF to estimate the illumination component.

2.2. Enhancing the Intensity Layer.

Generally, the processing of an RGB image is to operate the R, G, and B three channels separately, which is time-consuming. In this work, the low-light image is converted from RGB color space to HSI color space. The HSI color space stems from the human visual system, using three elements of color, hue (H), saturation (S), and intensity (I) to describe the color, which is more consistent with human visual feature than RGB color space. In HSI color space, the intensity component is enhanced while the hue and saturation components are extracted without further processing.

2.2.1. Estimating Illumination Component.

Based on illumination-reflection model, combined with (2), (4), and (15), we use the GDGIF to estimate the illumination

(a) Original image

(b) Image filtered by GIF

(c) Image filtered by WGIF

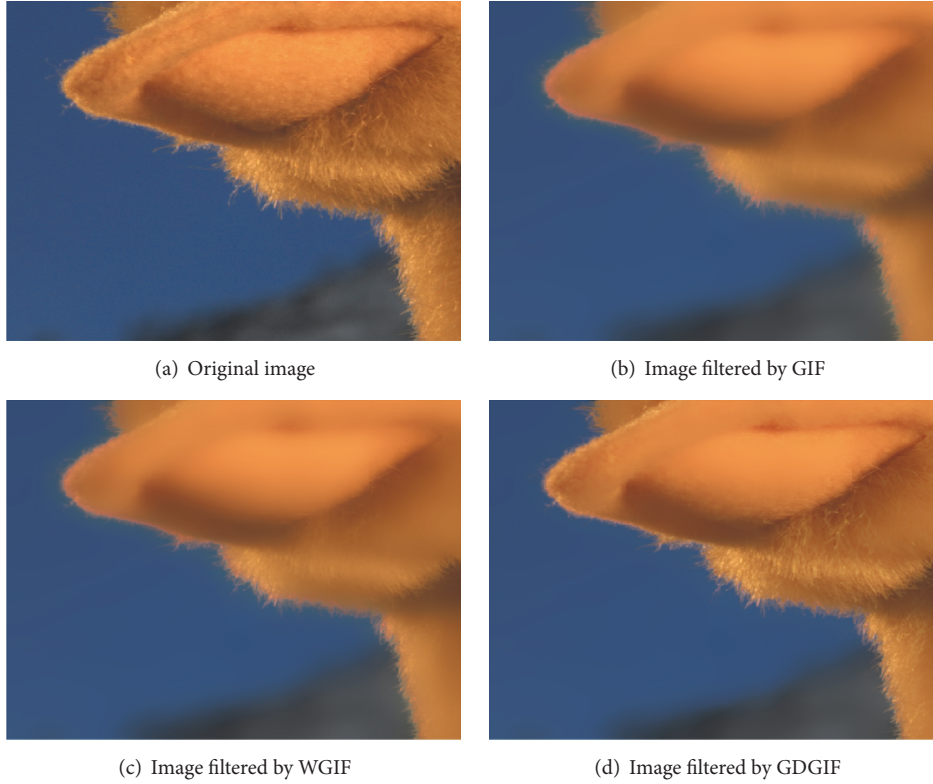(d) Image filtered by GDGIF

FIGURE 4: The difference between GIF, WGIF, and GDGIF.

component $L_I(x, y)$ of intensity layer image $I(x, y)$ as follows:

$$L_I(x, y) = q(x, y) * I(x, y), \tag{17}$$

where $q(x, y)$ is represented by the GDGIF function, as shown in (4). Then the reflection component $R_I(x, y)$ of intensity layer image can be obtained according to (3) and (17) as follows:

$$r_I(x, y) = \lg[R_I(x, y)]$$
$$= \lg[I(x, y)] - \lg[L_I(x, y)]. \tag{18}$$

2.2.2. Enhancing Illumination Component. Normally, the methods based on illumination-reflection model are to extract and then enhance the reflection component without considering the illumination component. Such processing leads to a lack of coordination between gray levels and yields color distortion. To cope with this problem, Wu et al. [13] proposed enhancing the reflection component together with the illumination component. Inspired by this idea, we process the illumination component by the nonlinear tensile sigmoid transform as shown in Figure 5. It is indicated in [22] that the sigmoid transform has the ability to sharpen images, highlight the local details, and stretch the image contrast.

The nonlinear tensile sigmoid transform is expressed in the following equations:

$$l_{\text{Sigmoid}}(x, y) = r_{\min} + \frac{r_{\max} - r_{\min}}{1 + e^{-a(r(x,y) - b \cdot (r_{\max} - r_{\min}))}},$$
$$l_{I\_\text{out}}(x, y) = l_I(x, y) \times l_{\text{Sigmoid}}(x, y), \tag{19}$$

where l_{Sigmoid} is self-defined sigmoid nonlinear function, whose range is $[0, 1]$, $r_{\min}$ and $r_{\max}$ represent the minimum and maximum values of reflection component, respectively, and $l_I(x, y)$ and $l_{I\_\text{out}}(x, y)$ are the initial and the enhanced illumination component, respectively. It is noted that there are two important parameters a, b in which the parameter a controls how an image is enhanced and the parameter b controls the contrast enhancement. Generally, a large value of a enhances an image greatly. On the other hand, a small value of b enhances the contrast of the dark regions, and a large value of b enhances the contrast of the light regions. Figure 6 shows examples by taking different parameters. In this study, the parameters a, b are selected as 2 and 0.004, respectively.

2.2.3. Enhancing the Reflection Component. It is known that human eyes are not sensible for high brightness difference but sensible for the small difference in low intensity. Thus, gamma transform [23] is normally employed to enhance the reflection component as follows:

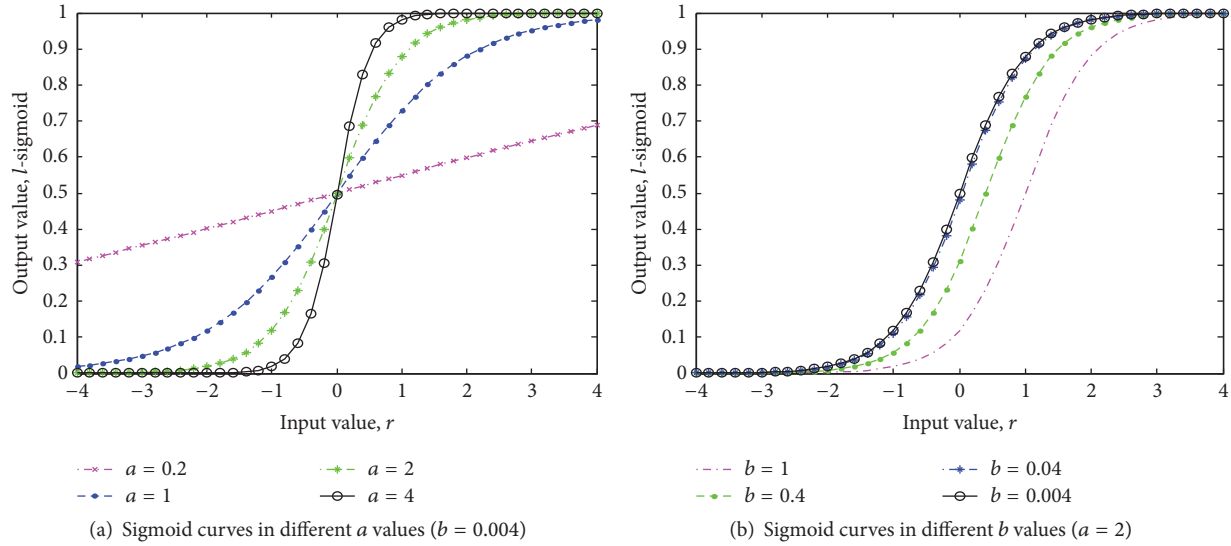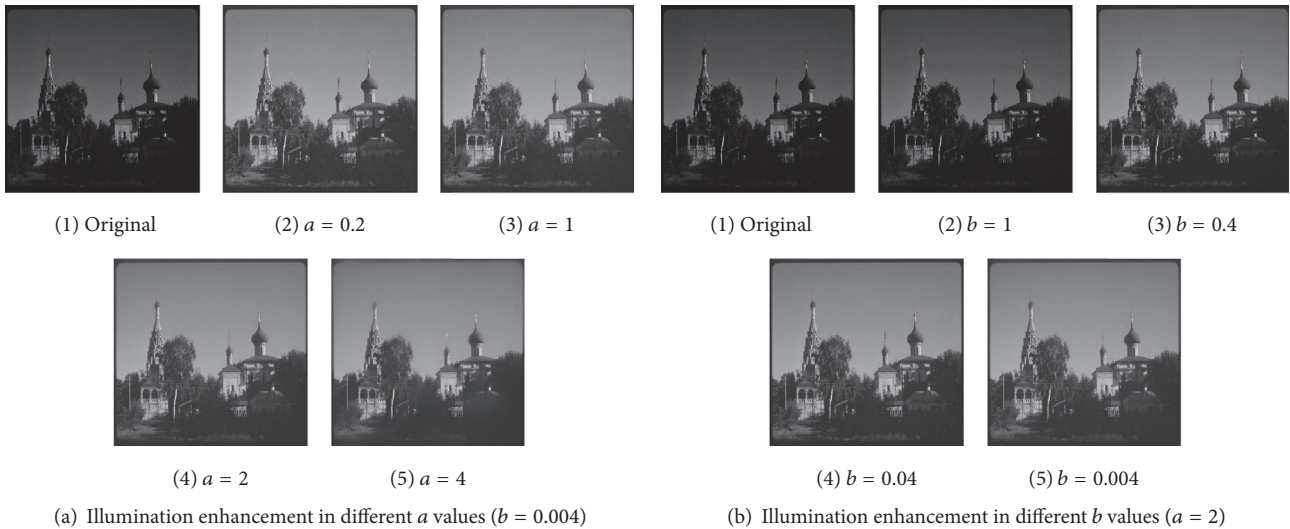$$r_{I\_\text{out}}(x, y) = c r_I^{\gamma}(x, y), \tag{20}$$

(a) Sigmoid curves in different a values ($b = 0.004$)

(b) Sigmoid curves in different b values ($a = 2$)

FIGURE 5: Sigmoid function curves.

(1) Original   (2) $a = 0.2$ (3) $a = 1$ (1) Original   (2) $b = 1$ (3) $b = 0.4$

(4) $a = 2$ (5) $a = 4$ (4) $b = 0.04$ (5) $b = 0.004$

(a) Illumination enhancement in different a values ($b = 0.004$)

(b) Illumination enhancement in different b values ($a = 2$)

FIGURE 6: Illumination component enhanced by sigmoid curves.

where c is a positive constant; γ is a parameter to control the image contrast.

It is seen from Figure 7 that when γ is less than 1, the contrast in low intensities is increased. On the contrary, the contrast in high intensities is enhanced in case $\gamma > 1$. The effect of parameter c is shown in Figure 8. In this work, the parameters are experimentally selected as follows: $\gamma = 0.6$; $c = 0.3$.

2.3. Final Enhanced Image. By taking antilog of the illumination component combined with the reflection component, we obtain the enhanced intensity image. The new HSI image is made up of enhanced intensity layer, original hue, and saturation layer. Then the enhanced HSI image is converted

into RGB image to obtain the final enhanced image. The whole process is shown in Figure 9.

3. Experimental Results and Discussions

As there is no public low-light image database, we collect 20 images from the Library of Congress and Internet as shown in Figure 10. In the simulation, the parameters are predefined as follows: window radius $r = 16$, regularization parameter $\varepsilon = 0.001$, the sigmoid parameters $a = 2$, $b = 0.004$, and gamma parameters $\gamma = 0.6$, $c = 0.3$. All experiments are performed in Matlab code on Windows 7 operation system. The computer is Intel® core™ i5-4570 3.20 GHz, and the RAM is 4.00 GB. The popular algorithms such as traditional
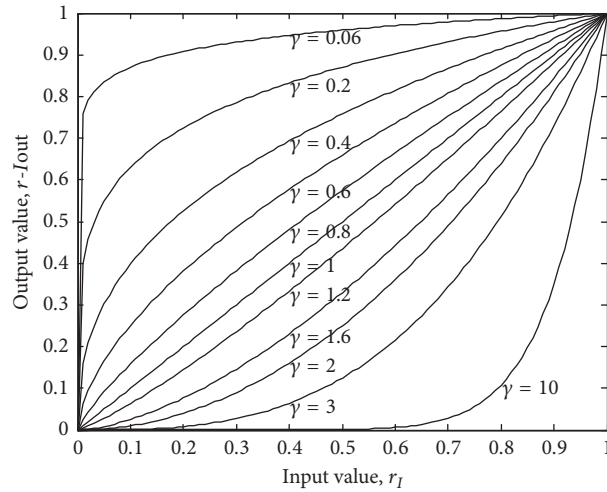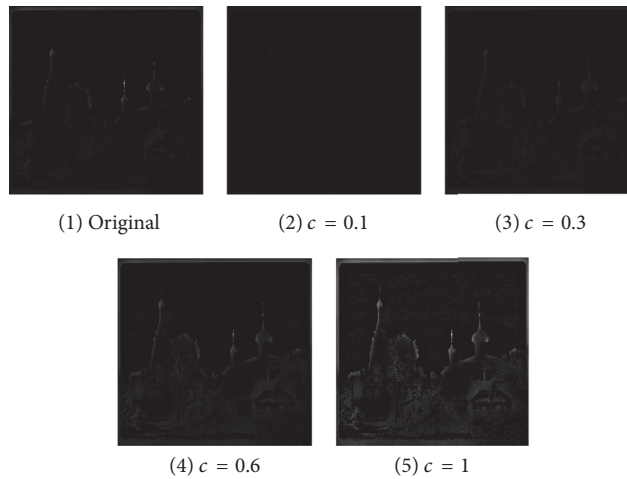
FIGURE 7: Gamma transforms ($c = 1$).

(1) Original   (2) $c = 0.1$ (3) $c = 0.3$

(4) $c = 0.6$ (5) $c = 1$

FIGURE 8: Reflection component enhanced by different c values.

MSR [11], Hao's algorithm [14], He's algorithm [17], histogram equalization (HE), improved MSR [12], and Kim's algorithm [9] are implemented for performance comparison.

3.1. Subjective Evaluation. It is observed from Figures 11 and 12 that the images enhanced by traditional MSR algorithm have obvious "white" phenomenon, which indicates color distortion. The images enhanced by Hao's method result in gradient reversal artefact as seen in red square from image 4 (white tower) in Figure 11, which indicates that the bilateral filtering has poor edge preserving property. Moreover, the resulting images by Hao's method are blurred which can be seen from images 1 (church) and 5 (the study) in Figure 11. He's algorithm also shows halo artefact which can be seen from image 1 (church), and this method cannot enhance the image contrast and brightness shown in Figure 12.

Histogram equalization algorithm can enhance image contrast, but this method misses details and enlarges noise, which can be observed from Figures 11 and 12. Improved MSR algorithm is better than the traditional MSR algorithm,

but this method causes halo artefact which can be seen from image 1 (church) in Figure 11 (highlighted box). Moreover, "white" phenomenon exists as shown in image 13 (boy), where the tire is over-enhanced and loses detailed information. Our results show that improved MSR algorithm is not effective in dealing with night images, as observed in Figure 12.

Kim's algorithm also causes color distortion, which can be seen from image 1 (church) in Figure 11, and the sky in the red square becomes gray. The enhanced images may be blurred as seen in image 1 (church), which implies that Kim's algorithm has poor edge preserving.

As seen from Figures 11 and 12, the proposed algorithm has the best color fidelity and edge preserving. Also, the enhanced images have less noise and clearer details than the one enhanced by histogram equalization algorithm.

3.2. Objective Evaluation. Currently, no standard objective metrics are proposed for enhancement assessment of low-light images. In this study, we employ information entropy

(a) Original

(b) Intensity layer image

(c) Illumination component

(d) Reflection component

(e) Enhanced illumination component

(f) Enhanced reflection component

(g) Enhanced intensity image

(h) Enhanced RGB image

FIGURE 9: The proposed procedure of low-light images.

(IE) to evaluate image details and choose the average edge intensity (AEI) to evaluate the edge preserving feature of enhanced images. The IE is defined as follows:

$$IE = -\sum_{s=0}^{L-1} P(r_s) \log_2 P(r_s), \qquad (21)$$

where $P(r_s)$ represents the probability of gray level s; L is the total number of gray levels. Larger IE indicates more

information, which implies that there are more details in the underlying image.

The AEI is defined as follows:

$$AEI = E(g(i,j)) = E\left(\sqrt{S_x(i,j)^2 + S_y(i,j)^2}\right), \qquad (22)$$

where $S_x(i,j)$ and $S_y(i,j)$ represent gradients in x and y directions on image edges. E represents expectation. In this study, Sobel operator is used for gradient computation. Larger
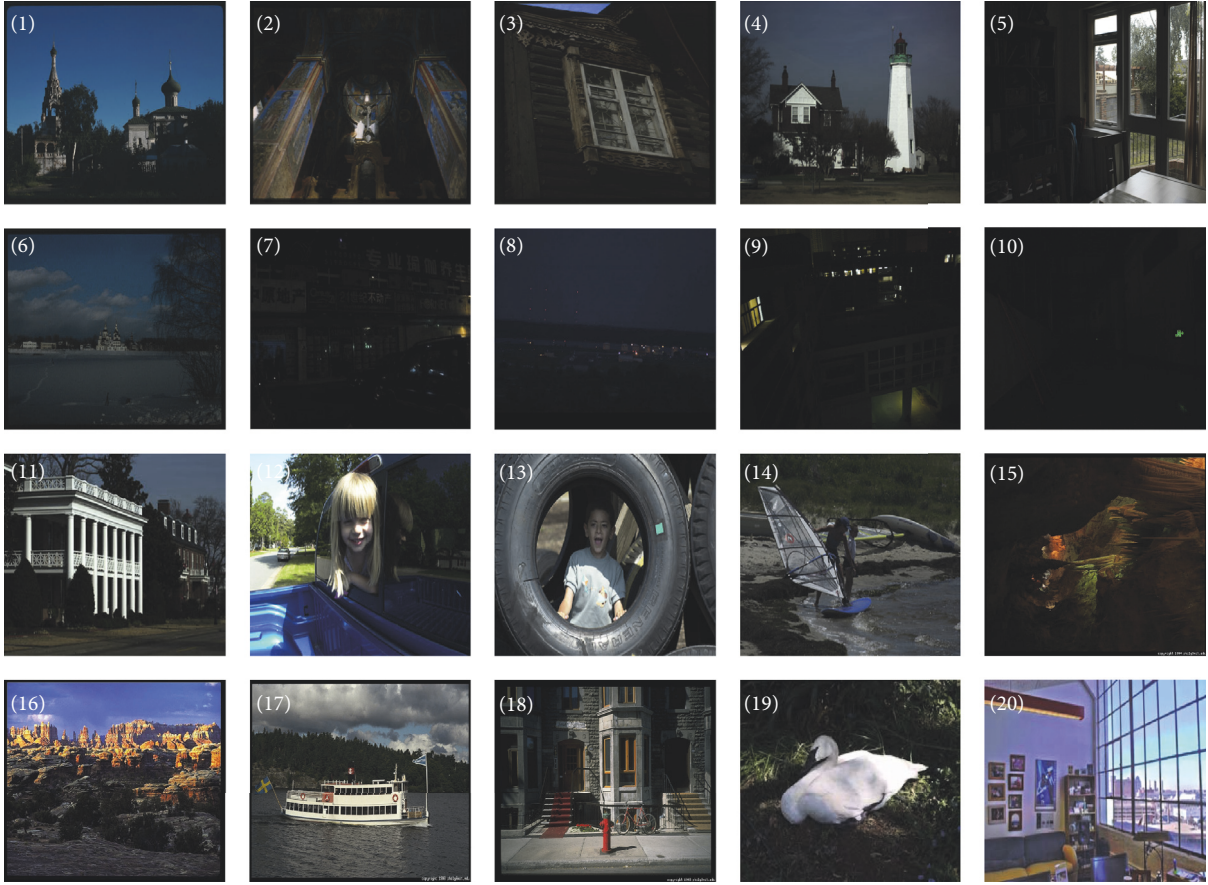
Figure 10: Datasets used in experiments.

AEI indicates good edge preserving. Also, the efficiency of the proposed method is compared with other methods.

Table 1 shows the average IE and AEI and operating time based on 20 test images. It is observed that the performance of He's method is not good in terms of IE. The images enhanced by He's method are usually dark and lose many details. Figure 13 shows the IE performances of the best three methods, that is, Hao's algorithm, Kim's algorithm, and the proposed method. It is seen that the median IE (marked by a red line) of the proposed method is the largest. The mean IE (marked by a green line) of the proposed method is 9.8% higher than Hao's algorithm and 1.8% higher than Kim's algorithm in the 20 test images.

On the other hand, it is observed from Table 1 that the improved MSR, histogram equalization (HE), Kim's algorithm, and the proposed algorithm achieve top four performances in terms of AEI. It is noted that high AEI in the histogram equalization accounts for much noise. The AEI of the improved MSR, Kim's method, and the proposed method on each individual image are shown in Figure 14. Results show that the median AEI (marked by a red line) of the proposed method is the largest, and the mean AEI (marked by a green line) of the proposed method is 26.8% higher than the improved MSR and 15.6% higher than Kim's algorithm.

Table 1: The average IE, AEI, and operating time (sec) on twenty images.

	Average IE	Average AEI	Average time
Original	11.057	50.756	N/R
Traditional MSR	13.439	67.485	1.77
Hao et al.'s [14]	14.091	57.838	16.289
He et al.'s [17]	11.867	61.952	0.377
HE	14.761	83.874	0.281
Improved MSR [12]	13.234	83.606	7.915
Kim et al.'s [9]	15.193	96.477	0.867
The proposed method	15.478	114.297	0.698

In summary, the proposed method achieves the best performance in terms of both IE and AEI. Furthermore,
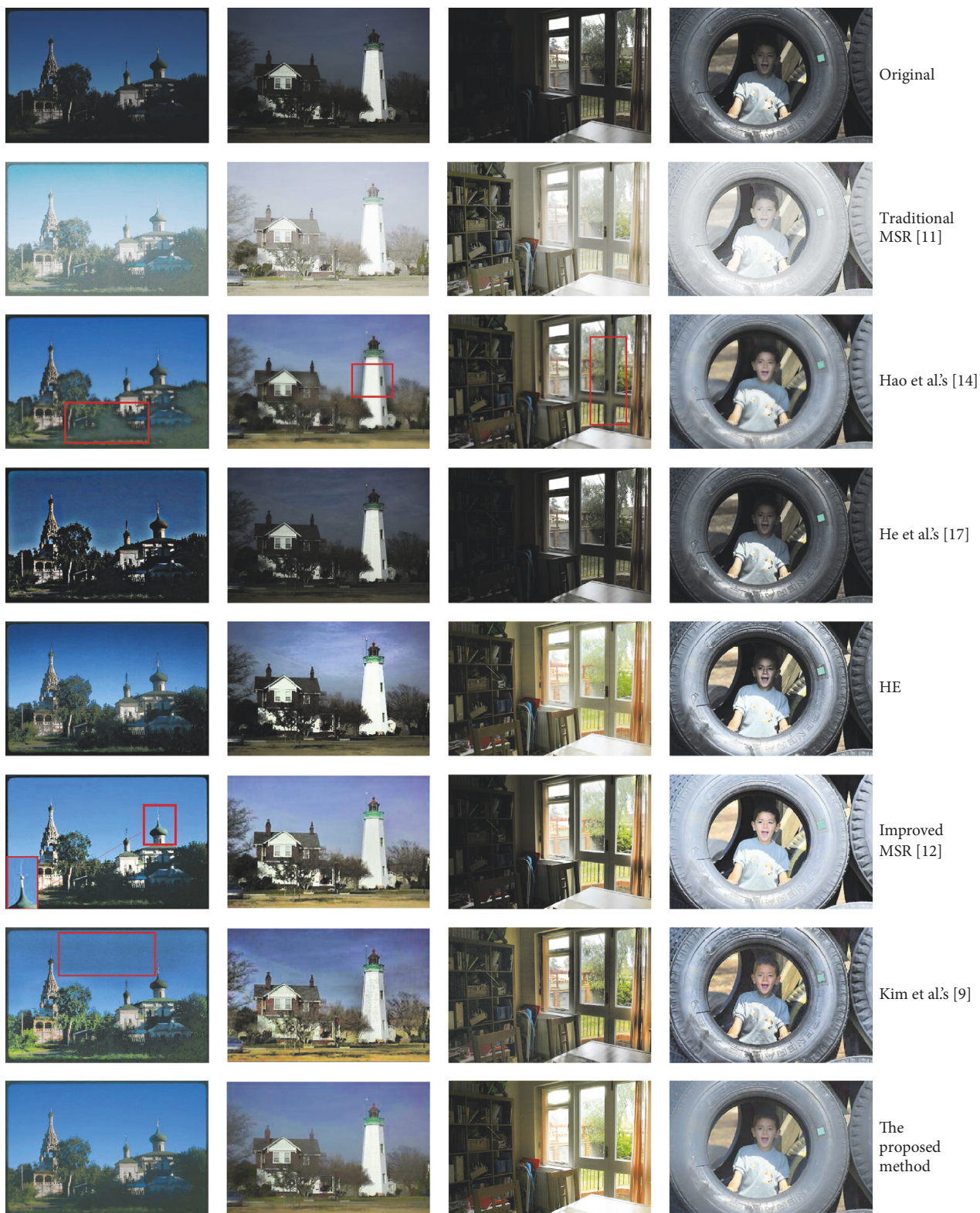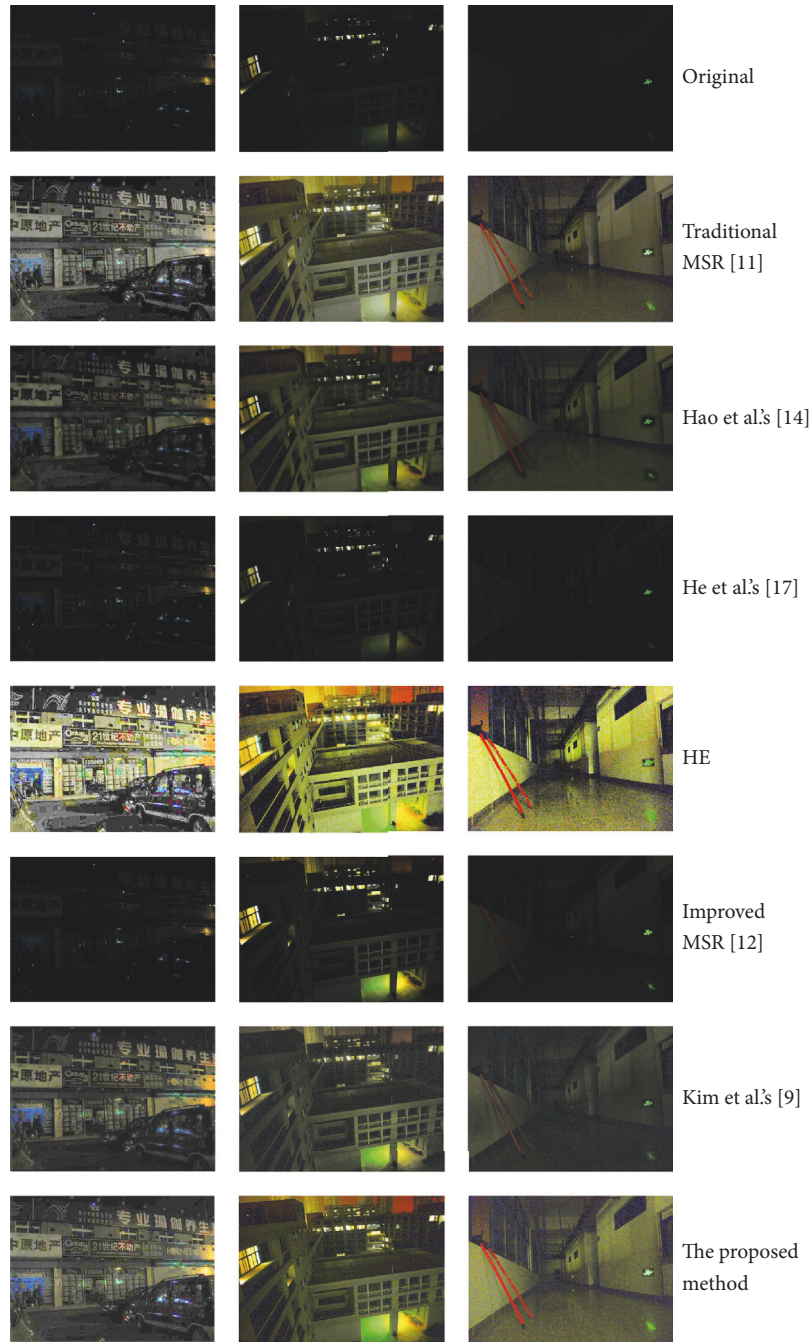
FIGURE 11: Comparison among different algorithms.

FIGURE 12: Results by different algorithms.

the proposed method is very efficient and achieves the 3rd position among the 7 methods as shown in Table 1. It is noted that He's algorithm has the worst enhanced image quality. Figure 15 shows the median operating time (marked by a red line) and the mean operating time (marked by a green line) of HE, Kim's, and the proposed method. Generally, the bilateral filtering is not as efficient as the GDGIF. The computation complexity of bilateral filtering is $o(Nr^2)$, where r refers to the window radius of bilateral filtering, and N is the number of image pixels while the GDGIF's computation complexity is

$o(N)$. In other words, the GDGIF's computation complexity is not related to the filter size. Results show that the average time by the proposed method is 59.7% higher than HE and 19.4% less than Kim's algorithm.

4. Conclusion

A low-light image enhancement algorithm is presented in the paper. By decomposing a low-light image into the illumination component and the reflection component, it
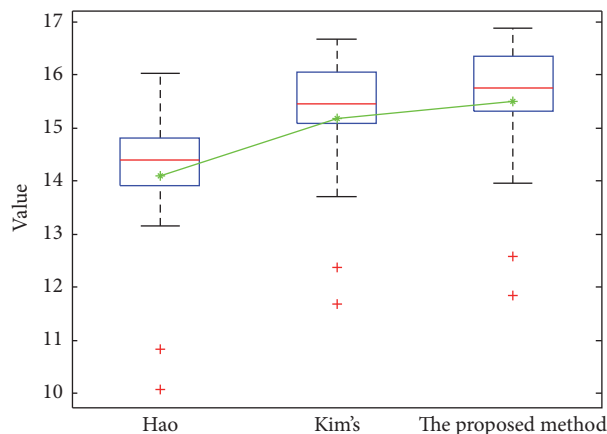
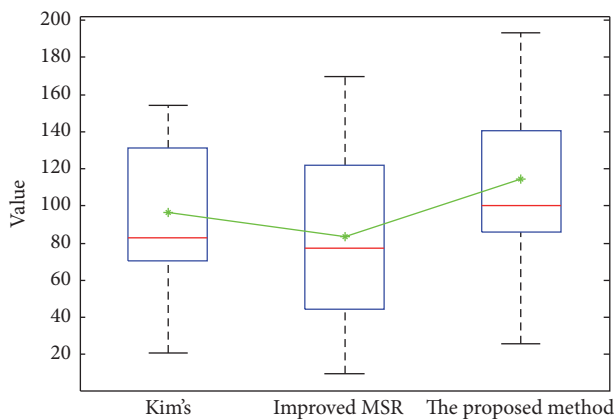FIGURE 13: IE results by Hao's, Kim's, and the proposed method.

FIGURE 14: AEI results by Kim's, improved MSR, and the proposed method.
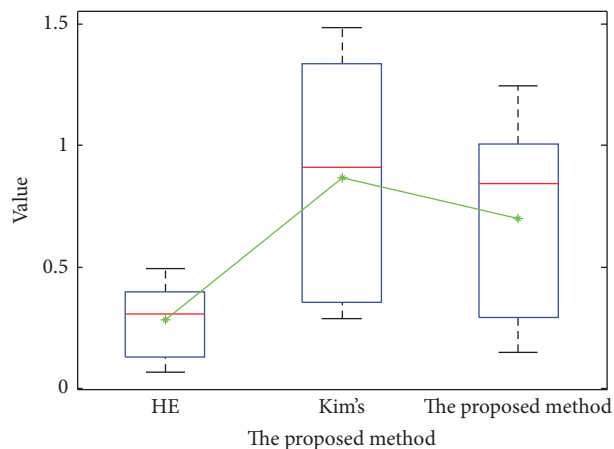

FIGURE 15: Operating time by HE, Kim's, and the proposed method.

offers a solution to expand illumination and enhances image details separately. Specifically, the illumination component is processed using guided image filter in gradient domain, followed by nonlinear sigmoid transform. The reflection component is enhanced by the gamma transform. This solution enhances low-light images and effectively avoids distortions

(for example color) and annoying artefacts (e.g., blurring, halo). Then, the final result is obtained by antilogging the sum of the enhanced two components. Experimental results demonstrate that the enhanced images by the proposed method are visually pleasing by subjective test and the performance of the proposed method outperforms the existing methods in terms of both IE and AEI assessments. Moreover, the proposed algorithm is efficient because the computation complexity is not related to filter size. The proposed method has great potential to implement in real-time low-light video processing.

Conflicts of Interest

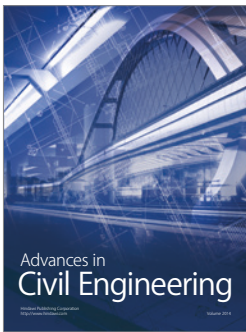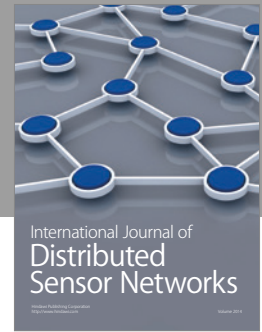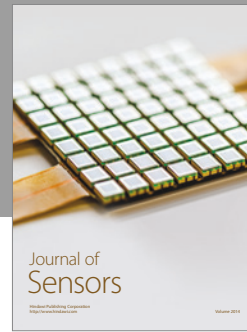The authors declare that they have no conflicts of interest.

Acknowledgments

References

[1] A. Alajarmeh, R. A. Salam, M. F. Marhusin, and K. Abdulrahim, "Real-time video enhancement for various weather conditions using dark channel and fuzzy logic," in *Proceedings of the 2014 International Conference on Computer and Information Sciences, ICCOINS 2014*, mys, June 2014.

[2] X. Jiang, H. Yao, S. Zhang, X. Lu, and W. Zeng, "Night video enhancement using improved dark channel prior," in *Proceedings of the 2013 20th IEEE International Conference on Image Processing, ICIP 2013*, pp. 553–557, aus, September 2013.

[3] L. Tang, S. Chen, W. Liu, and Y. Li, "Improved Retinex image enhancement algorithm," in *Proceedings of the 2011 2nd International Conference on Challenges in Environmental Science and Computer Engineering, CESCE 2011*, pp. 208–212, chn, December 2011.

[4] M. Athimethphat and K. Kritayakirana, "Enhanced illumination balancing with neural network for improved degraded scanned text-photo images," in *Proceedings of the 8th Electrical Engineering/ Electronics, Computer, Telecommunications and Information Technology (ECTI) Association of Thailand - Conference 2011, ECTI-CON 2011*, pp. 983–986, tha, May 2011.

[5] G. Yadav, S. Maheshwari, and A. Agarwal, "Contrast limited adaptive histogram equalization based enhancement for real time video system," in *Proceedings of the 3rd International Conference on Advances in Computing, Communications and Informatics, ICACCI 2014*, pp. 2392–2397, ind, September 2014.

[6] Z. Rong, Z. Li, and L. Dong-Nan, "Study of color heritage image enhancement algorithms based on histogram equalization," *Optik*, vol. 126, no. 24, pp. 5665–5667, 2015.

[7] J. Xiao, H. Peng, Y. Zhang, C. Tu, and Q. Li, "Fast image enhancement based on color space fusion," *Color Research and Application*, vol. 41, no. 1, pp. 22–31, 2016.

[8] Z. Liu, E. Blasch, Z. Xue, J. Zhao, R. Laganiére, and W. Wu, "Objective assessment of multiresolution image fusion algorithms for context enhancement in Night vision: A comparative study," *IEEE Transactions on Pattern Analysis and Machine Intelligence*, vol. 34, no. 1, pp. 94–109, 2012.

[9] S. E. Kim, J. J. Jeon, and I. K. Eom, "Image contrast enhancement using entropy scaling in wavelet domain," *Signal Processing*, vol. 127, pp. 1–11, 2016.

[10] E. Provenzi and V. Caselles, "A wavelet perspective on variational perceptually-inspired color enhancement," *International Journal of Computer Vision*, vol. 106, no. 2, pp. 153–171, 2014.

[11] D. J. Jobson, Z.-U. Rahman, and G. A. Woodell, "A multiscale retinex for bridging the gap between color images and the human observation of scenes," *IEEE Transactions on Image Processing*, vol. 6, no. 7, pp. 965–976, 1997.

[12] A. B. Petro, C. Sbert, and J. Morel, "Multiscale Retinex," *Image Processing On Line*, vol. 4, pp. 71–88, 2014.

[13] S. Wu, Z. Hu, W. Yu, and J. Feng, "An improved image enhancement approach based on Retinex theory," in *Proceedings of the 2013 International Conference on Information Technology and Applications, ITA 2013*, pp. 67–71, chn, November 2013.

[14] W. Hao, M. He, H. Ge, C.-J. Wang, and Q.-W. Gao, "Retinex-like method for image enhancement in poor visibility conditions," in *Proceedings of the 2011 International Conference on Advanced in Control Engineering and Information Science, CEIS 2011*, pp. 2798–2803, chn, August 2011.

[15] E. Land, "The retinex," *American Scientists*, vol. 52, no. 2, pp. 247–264, 1964.

[16] C. Tomaci and R. Mabduchi, "Bilateral filtering for gray and color images," in *Proceedings of the Proceeding of the 6th IEEE International Conference Computer Vision*, pp. 839–846, Bombay, India, January 1998.

[17] K. He, J. Sun, and X. Tang, "Guided image filtering," *IEEE Transactions on Pattern Analysis and Machine Intelligence*, vol. 35, no. 6, pp. 1397–1409, 2013.

[18] Z. Li, J. Zheng, Z. Zhu, W. Yao, and S. Wu, "Weighted guided image filtering," *IEEE Transactions on Image Processing*, vol. 24, no. 1, pp. 120–129, 2015.

[19] F. Kou, W. Chen, C. Wen, and Z. Li, "Gradient domain guided image filtering," *IEEE Transactions on Image Processing*, vol. 24, no. 11, pp. 4528–4539, 2015.

[20] P. Bhat, C. L. Zitnick, M. Cohen, and B. Curless, "GradientShop: A gradient-domain optimization framework for image and video filtering," *ACM Transactions on Graphics*, vol. 29, no. 2, article no. 10, 2010.

[21] M. Hua, X. Bie, M. Zhang, and W. Wang, "Edge-aware gradient domain optimization framework for image filtering by local propagation," in *Proceedings of the 27th IEEE Conference on Computer Vision and Pattern Recognition, CVPR 2014*, pp. 2838–2845, usa, June 2014.

[22] O. Nuri and C. Ender, "A non-linear technique for the enhancement of extremely non-uniform lighting images," *Journal of Aeronautics and Space Technologies*, vol. 3, no. 3, pp. 37–47, 2007.

[23] A. K. Bhandari, A. Kumar, and G. K. Singh, "Improved knee transfer function and gamma correction based method for contrast and brightness enhancement of satellite image," *AEU - International Journal of Electronics and Communications*, vol. 69, no. 2, pp. 579–589, 2015.

Journal of
Engineering

The Scientific World Journal

International Journal of
Rotating Machinery

Journal of
Sensors

International Journal of
Distributed
Sensor Networks

Advances in
Civil Engineering

Journal of
Control Science
and Engineering

Journal of
Robotics

Journal of
Electrical and Computer
Engineering

Hindawi

Submit your manuscripts at
https://www.hindawi.com

Advances in
OptoElectronics

VLSI Design

International Journal of
Navigation and
Observation

Modelling &
Simulation
in Engineering

International Journal of
Aerospace
Engineering

International Journal of
Chemical Engineering

International Journal of
Antennas and
Propagation

Active and Passive
Electronic Components

Shock and Vibration

Advances in
Acoustics and Vibration